

Global parameterization of $\pi\pi$ scattering up to 2 GeV

J. R. Pelaez,^{1,*} A. Rodas,^{1,†} and J. Ruiz de Elvira^{2,‡}

¹*Departamento de Física Teórica and IPARCOS, Universidad Complutense de Madrid, E-28040 Madrid, Spain*

²*Albert Einstein Center for Fundamental Physics, Institute for Theoretical Physics, University of Bern, Sidlerstrasse 5, 3012 Bern, Switzerland*

We provide global parameterizations of $\pi\pi \rightarrow \pi\pi$ scattering $S0$ and P partial waves up to roughly 2 GeV for phenomenological use. These parameterizations describe the output and uncertainties of previous partial-wave dispersive analyses of $\pi\pi \rightarrow \pi\pi$, both in the real axis up to 1.12 GeV and in the complex plane within their applicability region, while also fulfilling forward dispersion relations up to 1.43 GeV. Above that energy we just describe the available experimental data. Moreover, the analytic continuations of these global parameterizations also describe accurately the dispersive determinations of the $\sigma/f_0(500)$, $f_0(980)$ and $\rho(770)$ pole parameters.

I. INTRODUCTION

The unprecedented high statistics on hadronic observables attained at experiments like LHCb, Belle or Babar require rigorous and precise parameterizations of final state interactions. Future Hadronic facilities (Fair, Panda, etc..) will be even more demanding. One of the most needed parameterizations is that of $\pi\pi \rightarrow \pi\pi$ scattering, since two or more pions appear very frequently as final products of many hadronic interactions. In addition, a renewed interest on $\pi\pi \rightarrow \pi\pi$ scattering is coming from lattice calculations, which have been recently able to obtain scattering partial waves with almost realistic masses [1].

Data on $\pi\pi \rightarrow \pi\pi$ scattering was obtained in the 70's [2–6] indirectly from the $\pi N \rightarrow \pi\pi N$ reaction. Unfortunately, this technique gave rise to several conflicting data sets. Thus, for decades, crude models were enough to describe such data. The exception is the very low-energy region, both in the experimental and theoretical fronts. On the one hand, there is very precise data below the kaon mass coming from K_{l4} decays [7, 8], particularly after the NA48/2 results [9]. On the other hand, Chiral Perturbation Theory (ChPT) [10, 11] provides a systematic and accurate low-energy expansion in terms of pion masses and momenta.

However, for most phenomenological applications the low-energy region is not enough, since the production of pions is generically more copious around resonances. ChPT can be successfully extended to the resonance region by means of dispersion relations [12–15], usually called Unitarized ChPT. Different versions or approximations of this method generate or reconstruct all resonances in $\pi\pi \rightarrow \pi\pi$ up to 1.2 GeV: the $\sigma/f_0(500)$ the $\rho(770)$ and the $f_0(980)$ [16–20] and even in πK scattering. However, the prize to pay is the loss of a controlled systematic expansion, which hinders the calculation of uncertainties, and the length of the analytic expressions

once one deals with coupled channels above $K\bar{K}$ threshold. Above 1.2 GeV one can introduce by hand other resonances, yielding a successful description of data [21], although with the same caveats as before and with expressions even more elaborated. Nevertheless, the interest of these unitarized approaches is that they can connect with QCD through the chiral parameters and provide a good semi-quantitative approximation, including values of resonance poles, which are much better than the usual description of two pions in terms of simple popular models, like the superposition of simple resonant shapes, Breit-Wigner formulas in different versions, isobar models, etc...

The interest of those naive popular models is, on the one hand, their simplicity, since for most applications just the phase and the elasticity functions are needed, not an elaborated model of the interactions with other channels. On the other hand, they can be fairly reasonable for narrow isolated resonances, like the $\rho(770)$. However, such simple models provide an incorrect description of the scalar-isoscalar partial wave, particularly for the very broad $\sigma/f_0(500)$ pole and its interplay with the very narrow $f_0(980)$, together with the singularity structure in terms of cuts in the complex s plane. Actually, the rescattering of two pions in this channel is frequently described with some sort of Breit-Wigner parameterization for the $\sigma/f_0(500)$, which might be able to describe a wide bump in the data, but fails to describe the chiral constraints in the threshold region as well as the phase shift in the whole $\sigma/f_0(500)$ region. Recall that by Watson's Theorem [22] any strong elastic rescattering of two pions must have the very same phase of the $\pi\pi \rightarrow \pi\pi$ partial-wave with the same isospin and angular momentum.

In general, modern Hadron Physics demands more precise and model-independent meson-meson scattering parameterizations. This has been achieved over the last two decades by means of dispersion relations, not only for $\pi\pi$ [23–25], but also for πN [26, 27] or πK scattering [28]. Unfortunately, we have found that, for the hadron community, these dispersive results, either obtained numerically from complicated integral equations or parameterized by piecewise functions, are not always so easy to im-

* jrpelaez@fis.ucm.es

† arodas@ucm.es

‡ elvira@itp.unibe.ch

plement or do not cover a sufficiently large energy region. Hence, the purpose of this work is to provide relatively simple and ready-to-use parameterizations of the phase and elasticity of the scalar-isoscalar and vector $\pi\pi \rightarrow \pi\pi$ scattering partial waves up to almost 2 GeV. They will be consistent with data globally from threshold up to approximately 2 GeV, and with the dispersive analysis in [25], which extends up to 1.43 GeV in the real axis. Moreover, we will impose that these parameterizations will provide a simple analytic continuation to the complex plane, consistent with the dispersive representation and the values for the pole positions and residues of the $\sigma/f_0(500)$, $\rho(770)$ and $f_0(980)$ resonances found in [29]. In addition, both the dispersive results for the threshold and subthreshold regions are also described, thus providing the scattering lengths, slope parameters and S_0 wave Adler zero values obtained in [25].

II. THE INPUT TO BE DESCRIBED

As we already commented, there are several $\pi\pi \rightarrow \pi\pi$ scattering data sets extending up to almost 2 GeV [2–6]. These are customarily given in terms of partial waves t_ℓ^I of definite isospin I and angular momentum ℓ . We will also use the spectroscopic notation where the $\ell = 0, 1, 2, 3, \dots$ waves are referred to as S, P, D, F... waves, followed by their isospin. Unfortunately, all those data sets are often incompatible from one another and, moreover, simple fits to each separated set or to averaged data sets do not satisfy well dispersion relations [25, 30–33]. Nevertheless, it is possible to use dispersion relations as constraints to obtain a Constrained Fit to Data (CFD) [25] that still describes the $\pi\pi \rightarrow \pi\pi$ data on partial-waves but satisfies dispersion relations within uncertainties. Furthermore, the CFD fulfills the normality requirements of the residual distribution [34], hence ensuring that the standard approach for error propagation can be used. This CFD parameterization will thus be part of our input.

One might wonder why not using directly this CFD parameterization and why in this work we are trying to obtain another one. After all, this parameterization has become quite popular and it has been used in many phenomenological applications. There are several reasons.

First, the dispersion relations used in [25] are of two kinds and they were applied up to different energies, always below 2 GeV. One kind consists of a set of Forward Dispersion Relations, which were studied up to 1.43 GeV. These equations are rather simple, but unfortunately cannot be extended to the complex plane in search for poles. They are only useful as constraints on the real axis. The other kind consists of two sets of partial-wave dispersion relations, usually referred to as Roy equations [23, 24, 35] (with two subtractions) and GKPY equations [25] (with one subtraction). The former are more stringent in the low-energy region and the latter in the resonance region. Unfortunately, these

partial-wave equations are limited to 1.12 GeV, although they can be rigorously continued to the complex plane in search for resonance poles. The existence of these different energy regions motivated the authors in [25] to describe the data with a piecewise parameterization, which in principle cannot be extended rigorously to the complex plane. Therefore, our first aim is to provide a rather simple but global analytic parameterization, with realistic uncertainties, that can be used from $s = 0$ to 1.43 GeV. Thus, it will mimic the CFD piecewise parameterization *in the real axis*, which will be used as the first of our inputs to be described.

Second, the $\sigma/f_0(500)$ pole lies so deep in the complex plane that a careful dispersive determination is needed in order to extract its precise parameters rigorously [29, 36, 37]. Using the CFD parameterization as input in the GKPY equations, it was obtained numerically that its pole lies at $\sqrt{s_\sigma} = (457_{-13}^{+14}) - i(279_{-7}^{+11})$ MeV with a residue $|g| = 3.57_{-0.13}^{+0.11}$. Now, the low-energy piece of the CFD parameterization [25] was constructed as a conformal expansion valid up to 850 MeV, which lies within the elastic $\pi\pi \rightarrow \pi\pi$ region. This CFD conformal piece can be continued to the complex plane finding $\sqrt{s_\sigma} = (474 \pm 6) - i(254 \pm 4)$ MeV, which is fairly close, but it is not the pole obtained from the dispersive representation. This discrepancy does not improve when one includes further constraints in the real axis. Namely, even if the CFD conformal parameterization is extended up to the $K\bar{K}$ threshold to take into account the $f_0(980)$ effect or to the subthreshold region, in order to describe the dispersive value for the Adler zero, one still finds sizable discrepancies with the GKPY pole result. This problem was observed time ago [38–41]; arbitrarily small changes in the real axis input data may lead to indefinitely large variations for the analytic continuation to the complex plane. This illustrates how trying to obtain the $\sigma/f_0(500)$ pole from a data fit that only reaches 850 MeV is not precise enough. Actually, the effects of the $f_0(980)$ and other singularities, like the left hand cut, are significant at this level of precision. Hence, our second aim is to provide a simple analytic parameterization that reproduces simultaneously the dispersive poles of the $\sigma/f_0(500)$ and $f_0(980)$ and their interference. Thus, the numerical results of the GKPY dispersion relations in the complex plane, including the numerical values of the $\sigma/f_0(500)$ and $f_0(980)$ poles, will be the second input to be described. For the P -wave we will proceed similarly, but just for the $\rho(770)$ pole.

Finally, the CFD parameterization and the dispersive data analysis from which it was obtained only reach 1.43 GeV, but there are more data up to almost 2 GeV. However, the data at those high energies have many well-known caveats. Some of them were already discussed in detail in [42] and in appendix C of [30], but we summarize them here. First, in that energy region we have to rely on a single scattering experiment, the CERN-Munich Collaboration, so that systematic uncertainties relative to other experiments are not available. Second, this collab-

oration has many different solutions for the $\pi\pi$ scattering partial waves. Of these, the most popular one for the S0-wave is the one published in 1973 [2], also called “solution b” in the collaboration compilation of Grayer et al. [3]. This solution is also consistent with a later reanalysis with polarized targets [5]. In addition, there is the “solution (- - -)”, which was the most favored in the 1975 collaboration reanalysis [4] and the most used solution for the P-wave. Note that both “b” and “(- - -)” solutions are compatible with one another below 1.43 GeV. Other solutions for both waves were already disfavored in that very same analysis. Third, both solutions have caveats. On the one hand, the inelastic contribution to all hadronic cross sections are expected to dominate over the elastic ones (something that has been verified for πN , KN and NN scattering). However, this is not the case of “solution b”. It is hard to understand why this should be different for pions. On the other hand, if the inelasticity is large, then it can be proved theoretically [43, 44] that the solution in terms of phase and elasticity is not unique. “Solution b” is an example of an almost elastic case and “solution (- - -)” of a strong inelastic effect. Finally, the very same convergence of the partial-wave expansion could be questioned at those energies, since around 1.7 GeV the F-wave is as large as the P-wave, the D0 wave as large as the S0 and the D2 actually larger than the S2.

Therefore, in view of the caveats above, we have extended our fits beyond 1.43 GeV using as our third source of input, either the data of [2, 3, 5], which reaches up to 1.9 GeV, to obtain a “solution I” or the (- - -) data of [4], which reaches up to 1.8 GeV, to obtain a “solution II”. Below 1.43 GeV the input is the same for both our solutions and they agree within uncertainties. As a technical remark, we have ensured that the central value and the first derivative of both the phase and elasticity are continuous at the matching point, which is chosen at 1.4 GeV to avoid fitting the very end of the CFD parameterization. In any case, one should keep in mind that neither one of these two solutions has been checked against dispersion relations above 1.43 GeV. Thus, beyond that energy they should be considered purely phenomenological data fits.

III. ANALYTIC PARAMETERIZATIONS

In this section we present the parameterizations used for the scalar-isoscalar and vector $\pi\pi \rightarrow \pi\pi$ partial waves. Let us first note that below the $K\bar{K}$ threshold the process will be considered elastic and hence it will be uniquely characterized by its phase shift $\delta_\ell^I(s)$, as it is customary, through the following definition:

$$t_\ell^I(s) = \frac{\hat{t}_\ell^I(s)}{\sigma(s)} = \frac{e^{i\delta_\ell^I(s)} \sin \delta_\ell^I(s)}{\sigma(s)} = \frac{1}{\sigma(s)} \frac{1}{\cot \delta_\ell^I(s) - i}, \quad (1)$$

where $\sigma(s) = 2q(s)/\sqrt{s} = \sqrt{1 - 4m_\pi^2/s}$ is the two-pion phase space. The elastic region will be described with

conformal maps for both the S and P waves.

Let us also recall here the standard inelastic partial-wave representation

$$t_\ell^I(s) = \frac{\eta_\ell^I(s) e^{2i\delta_\ell^I(s)} - 1}{2i\sigma(s)}, \quad (2)$$

where the elasticity parameter $\eta_\ell^I(s)$ and phase shift will be described by two independent functions. However, note also that we will deal differently with the scalar and the vector elasticity. The reason is the presence of the $f_0(980)$ resonance in the scalar wave, which makes the elasticity rather small very near $K\bar{K}$ threshold, whereas the P wave remains almost elastic up to 1.4 GeV. In particular, it will be convenient to factorize the $f_0(980)$ effects from other contributions to the S0 wave elasticity.

Let us now describe separately the parameterizations we have used to describe the two partial waves of interest for this work.

A. S0-wave parameterization

As explained above, our parameterizations will be consistent with the dispersive data analysis of [25], which extends up to 1.43 GeV. Above that we will only provide two phenomenological fits to two sets of incompatible data, carefully matched to our parameterizations below. Let us discuss both regions separately.

1. S0-wave parameterization below 1.4 GeV

The $\sigma/f_0(500)$ and $f_0(980)$ resonances dominate the behavior of the S0 partial wave in this region. The somewhat controversial $f_0(1370)$ couples very weakly to two pions and its effect in this region can be treated as background. For our purposes it is important to remark that the $\sigma/f_0(500)$ has an associated pole very deep in the complex plane that produces a wide structure increasing monotonously from threshold up to roughly 900 MeV, reaching a phase-shift of 90° around 800 MeV, as seen in Fig.1. It is known [33] that the $\sigma/f_0(500)$ pole can be generated in the S0 partial wave by a simple truncated conformal expansion, that we will call $t_{0,\text{conf}}^0(s)$. However, above 900 MeV the $f_0(980)$ pole adds a further sharp increase that makes the phase larger than 200° right below the $K\bar{K}$ threshold. The phase then keeps growing slower but monotonously until 2 GeV.

It is worth noticing that the interplay between the $\sigma/f_0(500)$ and $f_0(980)$ poles produces a sharp dip in the modulus of the amplitude and the elasticity right above the $K\bar{K}$ threshold. In order to describe the $f_0(980)$ effects accurately and consistently with the dispersive results, we will factorize in the S matrix the $f_0(980)$ shape separately from the conformal expansion that contains

the $\sigma/f_0(500)$ pole. This means $S_0^0 = S_{f_0}^0 S_{0,\text{conf}}^0$, where

$$\begin{aligned} S_0^0 &= 1 + 2i\sigma(s)t_0^0, \\ S_{0,\text{conf}}^0 &= 1 + 2i\sigma(s)t_{0,\text{conf}}^0, \\ S_{f_0}^0 &= 1 + 2i\sigma(s)t_{f_0}^0. \end{aligned} \quad (3)$$

This factorization ensures elastic unitarity for the S0 wave, i.e. $|S_0^0| = 1$, when both the conformal and the $f_0(980)$ contributions fulfill elastic unitarity independently, i.e. $|S_{0,\text{conf}}^0| = |S_{f_0}^0| = 1$. This will be the case in the elastic region below the $\bar{K}\bar{K}$ threshold, $s < 4m_K^2$.

For our purposes, we are interested in the amplitude partial-wave

$$t_0^0(s) = t_{0,\text{conf}}^0(s) + t_{f_0}^0(s) + 2i\sigma(s)t_{0,\text{conf}}^0 t_{f_0}^0(s). \quad (4)$$

Now, the conformal factor of the partial wave is built by analogy to the elastic formulation in Eq. (1)

$$t_{0,\text{conf}}^0(s) = \frac{1}{\Psi(s) - i\sigma(s)}, \quad s < 1.4 \text{ GeV} \quad (5)$$

where, building on [33]

$$\Psi(s) = \frac{m_\pi^2}{s - z_0^2/2} \left(\frac{z_0^2}{m_\pi \sqrt{s}} + \sum_{n=0}^N B_n \omega(s)^n \right). \quad (6)$$

Let us remark that $\Psi(s) = \sigma(s) \cot \delta_0^0(s)$ in the elastic region $s \leq 4m_K^2$, implying $|S_{0,\text{conf}}^0| = 1$. The $s - z_0^2/2$ denominator provides the so-called Adler zero at $s_{\text{Adler}} = z_0^2/2$ required by chiral symmetry [45]. For $z_0 = m_\pi$ one would recover the Current-Algebra result, namely the leading order ChPT value. However, for us it will be a free parameter, fundamental to describe the subthreshold region. As we will see, it comes out from the fits consistent with the dispersive evaluation, which in turn is consistent with higher order ChPT evaluations (see [25, 46]). Note also that a term $\sim 1/\sqrt{s}$ is added to remove spurious poles or ghosts. As explained in [33] these ghosts are mostly harmless and have little relevance in the fit quality and the pole positions, but as a matter of principle it is better to remove them. As shown below, for this wave it will be enough to set $N = 5$ to obtain a good overall $\chi^2/d.o.f.$ in the elastic region.

The conformal variable is defined as

$$\omega(s) = \frac{\sqrt{s} - \alpha \sqrt{s_0 - s}}{\sqrt{s} + \alpha \sqrt{s_0 - s}}, \quad (7)$$

where s_0 corresponds to the highest value of s where the expansion is real and then α sets the center of the conformal expansion. We have found that the S0 wave is more conveniently described if the conformal expansion, by becoming imaginary, introduces some inelasticity above the $\bar{K}\bar{K}$ threshold [38]). Thus, we choose $s_0 = 4m_K^2$ with $\alpha = 1$ for simplicity, so that the expansion center lies near 0.7 GeV. Hence, between $\bar{K}\bar{K}$ threshold and 1.4 GeV, the $\Psi(s)$ function will be complex, which effectively introduces an inelasticity.

The unitarity of $t_{f_0}^0$ for $s < 4m_K^2$ is guaranteed by using

$$t_{f_0}^0(s) = \frac{sG}{M - s - \bar{J}(s, m_\pi) sG - \bar{J}(s, m_K) f(s)}, \quad (8)$$

which is inspired in the expression used in [38]. The \bar{J} loop functions are defined as

$$\bar{J}(s, m) = \frac{2}{\pi} + \frac{\sigma(s)}{\pi} \log \left(\frac{\sigma(s) - 1}{\sigma(s) + 1} \right). \quad (9)$$

Note that the constant G in the numerator in Eq. (8) is multiplied by s in order to cancel the phase-space pole at $s = 0$ in Eq. (4). In addition, this factor suppresses the inelastic contribution at low energies, hence ensuring that the low-energy region is dominated by the conformal parameterization. In principle, $f(s)$ could be any real analytic function and for convenience we will build it as an expansion of Chebyshev polynomials. The main advantage of this procedure is the low correlation among parameters, which will provide a more realistic description of the uncertainties. Note that the expansion variable will not be s , but a linear transformation that maps the $[2m_K, 1.5 \text{ GeV}]$ energy region into the $[-1, 1]$ segment, where Chebyshev polynomials are orthogonal. This variable is:

$$\omega_1(s) = 2 \frac{\sqrt{s} - 2m_K}{1.5 \text{ GeV} - 2m_K} - 1. \quad (10)$$

Thus, the real function $f(s)$ will be expanded as

$$f(s) = \sum_{i=0}^N K_i x_i(\omega_1(s)), \quad (11)$$

where x_i is the Chebyshev polynomial of order i . In practice it is enough to set $N = 3$ and so we will do. This function also suppresses the $f_0(980)$ contribution far from its nominal mass.

In practice, one can get acceptable $\chi^2/d.o.f.$ using Eq. (8) to fit the dispersive results in the real axis and the complex plane around the $\bar{K}\bar{K}$ threshold. However, when so doing the $f_0(980)$ pole position does not come out at the precise dispersive value given in [25]. For this reason we will impose the dispersive value of its pole position in the fit, by fixing the G, M constants.

Let us then briefly recall how to reach the second Riemann sheet in search for poles. According to the S -matrix unitary relation $SS^\dagger = \mathbb{1}$ and taking into account the Schwartz reflection symmetry, $t_\ell^I(s + i\epsilon) = t_\ell^I(s - i\epsilon)^*$, the partial wave second Riemann sheet $t_\ell^{2,I}$ is algebraically related to itself in the first Riemann sheet by

$$t_\ell^{2,I}(s) = \frac{t_\ell^I(s)}{1 + 2i\sigma(s)t_\ell^I(s)}, \quad (12)$$

where the $\sigma(s)$ determination is chosen so that $\sigma(s^*) = -\sigma(s)^*$ to ensure the Schwartz reflection symmetry

$$t_\ell^{2,I}(s^*) = t_\ell^{2,I}(s)^*. \quad (13)$$

As a consequence, a pole $s_p = s_R + is_I$ in the second Riemann sheet implies that a zero of the S matrix exists

$$M = \frac{(f_I J_{KR} + f_R J_{KI})(s_I(J_{\pi I} - 2\sigma_R) - s_R(J_{\pi R} + 2\sigma_I)) + (J_{\pi I} - 2\sigma_R)(s_I^2 + s_R^2)}{d} - (f_I J_{KI} - f_R J_{KR}),$$

$$G = -\frac{f_I J_{KR} + f_R J_{KI} + s_I}{d}, \quad (14)$$

where we have defined the constants

$$\begin{aligned} f(s_p) &= f_R + i f_I, \\ \bar{J}(s_p, m_K) &= J_{KR} + i J_{KI}, \\ \bar{J}(s_p, m_\pi) &= J_{\pi R} + i J_{\pi I}, \\ \sigma(s_p) &= \sigma_R + i \sigma_I \\ d &= J_{\pi I} s_R + J_{\pi R} s_I + 2(\sigma_I s_I - s_R \sigma_R), \end{aligned} \quad (15)$$

and $s_p = s_R + is_I$ corresponds to the $f_0(980)$ pole position, which is therefore a parameter to be varied within its uncertainties in our formulas.

In summary, for the scalar wave below 1.4 GeV we will use Eq. (4) with $t_{f_0}^0(s)$ defined in Eqs. (8), (9) and (14), whereas $t_{0,\text{conf}}^0(s)$, containing the $\sigma/f_0(500)$ pole, is defined in Eqs. (5), (6), which above $K\bar{K}$ threshold gives and additional contribution to the inelasticity besides that of $t_{f_0}^0$.

2. S0-wave parameterization above 1.4 GeV

As we have emphasized repeatedly, from 1.43 GeV there are no dispersive data analyses and, besides, the data can be grouped into two inconsistent data sets. However, we are frequently asked if we could extend our parameterization beyond 1.43 GeV. Thus, we will provide simple phenomenological fits to the two sets of data that we will match to our formulas below 1.4 GeV so that the whole parameterization and its derivative are continuous. For this we need the values at $s_m = (1.4 \text{ GeV})^2$ of the phase shift, the elasticity and their derivatives with respect to the energy squared, denoted with a prime. These inputs will be taken from the parameterizations below 1.4 GeV.

To reduce the number of parameters, we will make use again of Chebyshev polynomials to describe the phase shift above s_m , namely

$$\begin{aligned} \delta_0^0(s) &= \delta_0^0(s_m) + \Delta_0^0[x_1(\omega_2(s)) + 1] + d_0[x_2(\omega_2(s)) - 1], \\ \Delta_0^0 &= \frac{\delta_0^0(s_m) - d_0 x_2'(-1)}{x_1'(-1)}. \end{aligned} \quad (16)$$

In practice, we will need just two Chebyshev polynomials. The presence of $\delta_0^0(s_m)$ ensures the continuity of the

also in the first Riemann sheet at s_p . This imposes two constraints on Eq. (8), which allow us to fix G and M as follows:

parameterization and the value of Δ_0^0 the continuity of the derivative. Therefore there is only one free parameter for the fit, d_0 . The value of δ_0^0 will be kept fixed to the central value when calculating uncertainties. This means that although the derivative is continuous, the uncertainties on the derivative at that point might have a small kink. Otherwise the error band becomes unrealistically large. The variable for the Chebyshev polynomials now is:

$$\omega_2(s) = 2 \frac{\sqrt{s} - \sqrt{s_m}}{2 \text{ GeV} - \sqrt{s_m}} - 1. \quad (17)$$

In contrast, the elasticity function will be fitted through an exponential function to ensure $1 \leq \eta_0^0 \leq 1$. We have found that in the case of the S -wave, Chebyshev polynomials in the exponent produce unwanted oscillations. Thus we will use a simple phenomenological expansion in terms of powers of $Q(s) \equiv q(s)/q_m - 1$, where $q_m = q(s_m)$. Explicitly:

$$\begin{aligned} \eta_0^0(s) &= \exp \left[- \left(\sqrt{-\log(\eta_0^0(s_m))} \right. \right. \\ &\quad \left. \left. - \frac{4q_m^2 Q(s) \eta_0^0'(s_m)}{\sqrt{-\log(\eta_0^0(s_m)) \eta_0^0(s_m)} + \sum_{k=0}^2 e_k Q(s)^2} \right)^2 \right]. \end{aligned} \quad (18)$$

Now three free parameters will be needed at most. Note that the logarithms in Eq. (24) appear in the constants needed for the smooth matching, but they do not introduce any spurious analytic structure. As with the phase, now η_0^0 will be kept fixed to its central value when calculating uncertainties.

Hence, the S0-wave high-energy parameterization has four free parameters, but we will see in practice that some of them can be fixed to zero for the fits.

B. P-wave parameterization

The $\pi\pi$ -scattering P -wave is completely dominated by the $\rho(770)$ meson, which is customarily described using simple resonance models, like variations of Breit-Wigner parameterizations. In many cases, this is fair enough.

However, even though the $\rho(770)$ is usually considered as the prototype of narrow resonance, its width is relatively large compared to its mass, which explains that the ρ -meson shape cannot be fully described with precision using a simple Breit-Wigner function or within an Isobar model, but requires additional shape parameters [47, 48]. Let us also recall that the $\rho(770)$ is the main player of vector meson dominance. Actually, it saturates the most common hadronic observables, like, for instance, the hadronic total cross section $\sigma(e^+e^- \rightarrow \text{hadrons})$, which implies applications well beyond low-energy meson physics. Thus, given its relevance for Hadron Physics, we will provide in this section an analytic parameterization to describe the $\pi\pi$ vector-isovector channel up to approximately 2 GeV.

This wave is much simpler than the S0, since the inelasticity sets in at much higher energies and is much smaller than for the S0 wave. Actually, there is no need to factorize explicitly any resonance pole in the inelastic region as we did for the $f_0(980)$. Nevertheless, we will still separate the energy regions below and above 1.4 GeV, because the latter is not tested against the dispersive representation and has two inconsistent data sets that will be fitted separately later.

1. P -wave parameterization below 1.4 GeV

This region is dominated by the $\rho(770)$ resonance and its peak mass will be imposed with an explicit factor in the conformal expansion that we will use to describe the phase shift in this whole region. Namely

$$\cot \delta_1^1(s) = \frac{\sqrt{s}}{2q^3(s)}(m_\rho^2 - s) \left(\frac{2m_\pi^3}{m_\rho^2 \sqrt{s}} + \sum_{n=0}^N B_n \omega(s)^n \right). \quad (19)$$

As with the S0 wave, the term $\sim 1/\sqrt{s}$ within the parenthesis removes spurious ghosts but makes an almost irrelevant contribution to the fit. For this wave it will be enough to set $N = 4$ to obtain a good overall $\chi^2/d.o.f$ in the elastic region. As before, the conformal variable is defined as

$$\omega(s) = \frac{\sqrt{s} - \alpha\sqrt{s_0 - s}}{\sqrt{s} + \alpha\sqrt{s_0 - s}}, \quad (20)$$

but now $s_0 = 1.43^2 \text{ GeV}^2$ and in order to get an error band whose shape is closer to the actual spread of data, α is chosen so that the expansion center is near the $\pi\pi$ threshold. Values ranging from 0.2 to 0.5 make a suitable parameterization and we use $\alpha = 0.3$.

We have already commented that, in contrast to the large $f_0(980)$ effects in the S0 wave, for the P -wave inelastic effects are negligible below $\sqrt{s_e} \equiv 1.12 \text{ GeV}$ and very small below $\sqrt{s_m} \equiv 1.4 \text{ GeV}$. Actually, in this range the elasticity in [25] is very smooth and compatible with

one within uncertainties. Thus, it will be enough to describe it with

$$\eta_1^1(s) = \begin{cases} 1 & s < s_e, \\ 1 - K_0(1 - s_e/s)^2 & s_e \leq s < s_m, \end{cases} \quad (21)$$

where K_0 is a constant to be determined by the fit. Using this phenomenological parameterization for the elasticity together with the conformal parameterization in Eq. (19) for the phase shift, we will manage to describe accurately both the real axis and complex plane of the P -wave, including the $\rho(770)$ pole, in the region below 1.4 GeV.

2. P -wave parameterization above 1.4 GeV

As before with the S0 wave, above $\sqrt{s_m} \equiv 1.4 \text{ GeV}$ we will provide just phenomenological fits to the P -wave data, ensuring a continuous matching for the phase and elasticity as well as their derivatives. The matching procedure is similar to that for the S0 wave.

For the P -wave the phase shift will be described using Chebyshev polynomials again. Once the matching with the previous parameterization below 1.4 GeV is implemented, the phase shift in this region reads:

$$\begin{aligned} \delta_1^1(s) &= \delta_1^1(s_m) + \Delta_1^1[x_1(\omega_2(s)) + 1] + d_0[x_2(\omega_2(s)) - 1] \\ &\quad + d_1[x_3(\omega_2(s)) - 1], \\ \Delta_1^1 &= \frac{\delta_1^1(s_m) - d_0x_2'(-1) - d_1x_3'(-1)}{x_1'(-1)}. \end{aligned} \quad (22)$$

Note that, compared to the S0 case, now we will need one more Chebyshev polynomial x_3 , leaving two degrees of freedom d_0 and d_1 for the P -wave phase above 1.4 GeV. The polynomials variable is the same as in the S0 case:

$$\omega_2(s) = 2 \frac{\sqrt{s} - \sqrt{s_m}}{2 \text{ GeV} - \sqrt{s_m}} - 1. \quad (23)$$

Also, as it happened in the S0 case, for the calculation of uncertainties we will keep $\delta_1^1(s_m)$ fixed to its central value.

Concerning the elasticity, we will use again an exponential to ensure $0 \leq \eta_1^1 \leq 1$, but this time Chebyshev polynomials are appropriate to describe the exponent:

$$\begin{aligned} \eta_1^1(s) &= \exp \left[- \left(\sqrt{-\log(\eta_1^1(s_m))} \right. \right. \\ &\quad \left. \left. + H_1^1(x_1(\omega_2(s)) + 1) + e_0(x_2(\omega_2(s)) - 1) \right. \right. \\ &\quad \left. \left. + e_1(x_3(\omega_2(s)) + 1) + e_2(x_4(\omega_2(s)) - 1) \right)^2 \right], \\ H_1^1 &= \frac{\eta_1^1(s_m) - e_0x_2'(-1) - e_1x_3'(-1) - e_2x_4'(-1)}{x_1'(-1)}. \end{aligned} \quad (24)$$

Note that the logarithms in Eq. (24) appear in the constants needed for the smooth matching but they do not

introduce any spurious analytic structure. The presence of the H_1^1 constant ensures the continuity of the derivative. For the calculation of uncertainties we will keep $\eta_1^1(s_m)$ fixed to its central value. Thus the central value of the derivative is continuous but its uncertainties might show a small kink.

IV. DETERMINATION OF PARAMETERS

The aim of this work is to provide a relatively simple global description for each one of the S0 and P waves of $\pi\pi \rightarrow \pi\pi$ scattering, incorporating all analytic constraints at low energies, including Adler zeros, while also describing the existing data up to 2 GeV. They should also be consistent with the dispersive analysis of data up to 1.4 GeV in [25]. Moreover, such parameterizations should provide also simple but realistic estimates of the uncertainties. In the previous section we have provided such simple and ready to use parameterizations. In this sections we will determine the value of their parameters.

Let us recall that the Constrained fit to Data (CFD) parameterizations of $\pi\pi \rightarrow \pi\pi$ scattering partial waves obtained in [25], were data fits constrained to fulfill a group of forward dispersion relations up to 1.43 GeV, together with the more sophisticated Roy and GKPY equations for the partial waves, applicable up to roughly 1.1 GeV. However they were parameterized with piecewise functions and we now want to mimic them and their uncertainties with a global parameterization. Thus, in the real axis the CFD partial waves of [25] will be fitted. The CFD has much smaller uncertainties than the output of the dispersion relations themselves, and this is why it is preferred to build a more accurate result. We will impose just the phase shift up to the inelastic $K\bar{K}$ threshold, and both the phase shift and elasticity above it.

In addition, we want our new parameterization to be consistent with the dispersive result in the complex plane, particularly with the resonance pole positions and residues. The CFD are piecewise functions and although some of the pieces contain fair approximations to the poles, they do not provide accurate results in the complex plane. Therefore below the elastic threshold, and in the complex plane, we will fit our global parameterization to the output of GKPY equations, which produces narrower errors than that of Roy equations, while both are compatible among themselves in the whole complex plane and real axis. The fit will run from about $\text{Re } s \sim (0 \text{ GeV})^2$ to $\text{Re } s \sim (1.12 \text{ GeV})^2$, but always inside the the applicability region of the GKPY or Roy dispersion relations, which can be found in [23, 35, 36]. Using such a vast region we are able to describe the scattering lengths, the Adler zeros in the S0 wave, and the $\sigma/f_0(500)$ and $\rho(770)$ pole positions and couplings, (the $f_0(980)$ is fixed as input). Due to the smaller uncertainties in the real axis, the final errors bars of our parameterization in the complex plane are smaller than the dispersive ones.

All these features will be imposed on our parameter-

ization by means of a $\chi^2/d.o.f.$ function, over a grid of points separated by 10 MeV both in the real and imaginary directions within the GKPY/Roy equations applicability region. The values and uncertainties in this χ^2 are those of the CFD in the real axis and of the GKPY output [25] in the rest of the complex plane. Nevertheless, the statistical meaning of the $\chi^2/d.o.f. \sim 1$ loses part of its purpose, as the results coming from dispersion relations are smooth functions instead of normally distributed points, and their uncertainties are totally correlated between bins. As a result, a value lower than 1 is frequently expected, and we will consider all results below or around 1 as good descriptions of our dispersion relations.

Finally, let us recall that above 1.43 GeV no dispersive result exists, thus we will make use of the available experimental data. The only sources of data in this energy region produce two different plausible solutions. The first one, called solution I in this work comes from [2, 3, 5, 49]. There is a second one, that we will call solution II, coming from a later reanalysis by the CERN-Munich collaboration [4].

A. S0-wave fit

Thus, we show in Fig. 1 the solutions I and II of our new S0-wave parameterization up to 1.9 GeV. Their parameters are listed in Table I for solution I and Table II for solution II. By construction, they are almost identical up to 1.4 GeV. Nevertheless, there is an almost imperceptible deviation between them in the inelastic region below 1.4 GeV due to their matching to different solutions above 1.4 GeV. Actually, above this splitting point the solutions are fairly different, in particular the elasticities display a clearly different pattern. It is worth noticing that the uncertainties of solution II are larger for the phase shift, due to the scarcity of data above 1.5 GeV. Furthermore, even though we included some data points coming from [2, 3] for the elasticity, solution II first drops and then raises in this region, which is hard to explain in terms of the known resonances. In contrast solution I slowly becomes more and more inelastic as the energy increases which is more natural if more and more channels are open.

Concerning the compatibility with the dispersive results in [25], we show in Fig. 2 the comparison between the CFD analysis of [25] and our solution I. An almost identical plot would be obtained for solution II, since they only differ significantly above 1.4 GeV. The relevant observation from Fig. 2 is that the piecewise CFD and our new parameterization look almost equal below the $K\bar{K}$ threshold and are also very similar and compatible above it. The sharp structure in the region between the two vertical lines in Fig. 2 is dominated by the $f_0(980)$ contribution that we have factored out explicitly in our global parameterization.

All in all, this new parameterization is consistent with

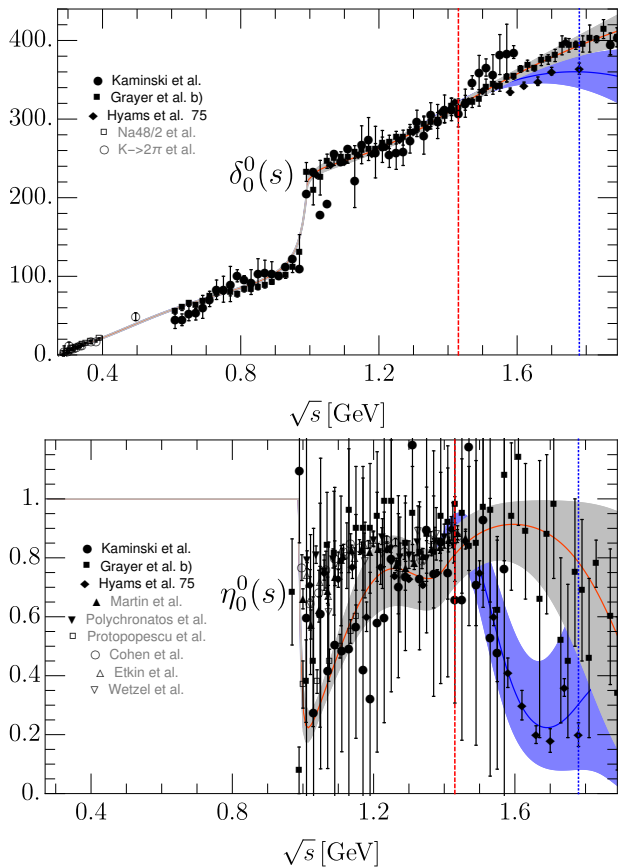


FIG. 1: Comparison of solutions I and II (Tables I and II) with data. Above 1.4 GeV, solution I fits the data of [5, 49] (solid circles) and [2, 3] (solid squares), whereas solution II fits [4] (solid diamonds). The data coming from [9] (empty squares), [50] (empty circles), [51] (triangle up), [52] (triangle down), [6] (empty squares), [50] (empty circles), [53] (empty triangle up) and [54] (empty triangle down) are just shown for comparison. The red-dashed vertical line separates the region where the fits describe both data and dispersion relation results from the region above, where the parameterization is just fitted to data. The blue-dotted vertical line depicts the energy of the last data point of solution II. The gray band corresponds to the uncertainty of solution I and the blue band to solution II.

the GPKY dispersive data analysis, its output in the complex plane, as well as with the threshold parameters, the Adler zero, the positions of both $\sigma/f_0(500)$ and $f_0(980)$ poles, and the inelastic region up to 1.43 GeV, which was consistent with Forward Dispersion Relations. This consistency is illustrated in Table III where we show the $\chi^2/d.o.f. \equiv \hat{\chi}^2$ of our fit with the new parameterization in different regions: $\hat{\chi}_1^2$ from $\pi\pi$ to $K\bar{K}$ threshold, $\hat{\chi}_2^2$ from $K\bar{K}$ threshold to 1.4 GeV, $\hat{\chi}_C^2$ in the complex plane within the applicability region, $\hat{\chi}_\delta^2$ for the phase above 1.4 GeV and $\hat{\chi}_\eta^2$ for the elasticity above 1.4 GeV. All of them are smaller or equal to one for any of our two

TABLE I: Fit parameters of the global parameterization for the S_0 -wave solution I. s_p is the $f_0(980)$ pole position from the dispersive analysis [29].

	$t_{0,\text{conf}}^0$	$t_{f_0}^0$	$\sqrt{s} > 1.4 \text{ GeV}$		
B_0	12.2 ± 0.3	K_0	1.29 ± 0.07	d_0	-5.4 ± 3.7
B_1	-0.9 ± 1.1	K_1	-1.08 ± 0.04	d_1	$\equiv 0$
B_2	15.9 ± 2.7	K_2	-0.043 ± 0.038	e_0	10.3 ± 4.0
B_3	-5.7 ± 3.1	K_3	-0.068 ± 0.015	e_1	$\equiv 0$
B_4	-22.5 ± 3.7			e_2	$\equiv 0$
B_5	6.9 ± 4.8	$\text{Re } \sqrt{s_p}$	0.996 ± 7		
z_0	0.137 ± 0.028	$\text{Im } \sqrt{s_p}$	-0.025 ± 8		

TABLE II: Fit parameters of the fits of the global parameterization for the S_0 -wave solution II. s_p is the $f_0(980)$ pole position from the dispersive analysis [29].

	$t_{0,\text{conf}}^0$	$t_{f_0}^0$	$\sqrt{s} > 1.4 \text{ GeV}$		
B_0	12.2 ± 0.3	K_0	1.22 ± 0.02	d_0	-16.5 ± 6.2
B_1	-1.2 ± 0.8	K_1	-1.16 ± 0.02	d_1	$\equiv 0$
B_2	15.5 ± 1.5	K_2	-0.010 ± 0.044	e_0	160.8 ± 2.4
B_3	-6.0 ± 1.5	K_3	-0.075 ± 0.010	e_1	-715.5 ± 8.5
B_4	-21.4 ± 1.3			e_2	-937.3 ± 25.0
B_5	6.3 ± 4.5	$\text{Re } \sqrt{s_p}$	0.996 ± 7		
z_0	0.135 ± 0.031	$\text{Im } \sqrt{s_p}$	-0.025 ± 8		

solutions.

TABLE III: Results in terms of $\hat{\chi}^2$ of the S_0 solution I and solution II in different regions.

	$\hat{\chi}_1^2$	$\hat{\chi}_2^2$	$\hat{\chi}_C^2$	$\hat{\chi}_\delta^2$	$\hat{\chi}_\eta^2$
Solution I	0.2	0.5	0.4	0.5	0.4
Solution II	0.2	0.5	0.3	1.0	1.0

1. Poles, Couplings and Low Energy Parameters

As explained above, the global parameterization is also constrained to describe the dispersive results in the whole complex energy-squared plane. This produces a stable and accurate description of the $\sigma/f_0(500)$ resonance parameters. Actually, in Fig. 3 we show our parameterization and its uncertainties in the first Riemann sheet of the complex plane, which reproduces the output of GPKY equations. In order to see the consistency with the GPKY dispersive result, in the upper panel of Fig. 4 we show the absolute values of the differences between the real part of our new parameterization and the GPKY result divided by the uncertainty of the latter. In the lower panel we show a similar plot for the imaginary parts. Note that our new parameterization lies within the uncertainties of the GPKY for the most part of the region. The only place where there are sizable differences

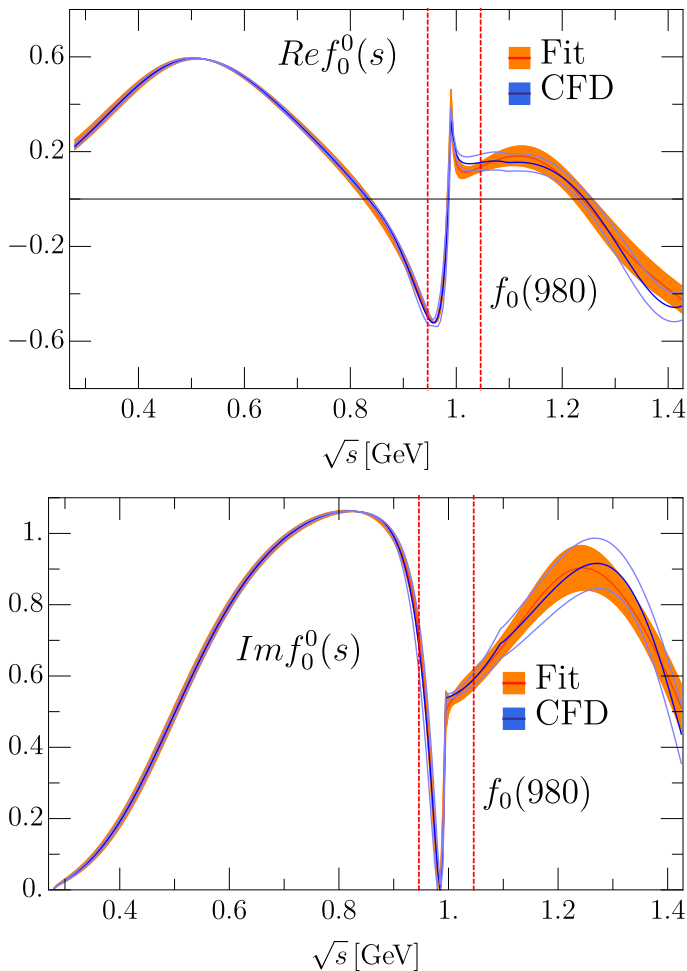


FIG. 2: Comparison between the CFD fit in [25] (blue) and solution I (Table I, orange band). The energy region dominated by the $f_0(980)$ pole is delimited between the red dashed lines.

beyond two standard deviations is for $\text{Im} t_0^0$ in the real axis around 0.9 GeV, but this is the matching point of the two pieces of the CFD parameterization, whereas the GKPY output is much smoother. Thus, our two inputs are slightly incompatible around that region and our new parameterization lies somewhere between both of them.

In addition, we list in Table IV the parameters of both the $\sigma/f_0(500)$ and $f_0(980)$ resonances compared to their GKPY dispersive values in [25]. It is worth noticing that the uncertainties of the $\sigma/f_0(500)$ resonance associated to this fit are a bit smaller than the GKPY determination [29]. This is due to the fact that besides the GKPY output in the complex plane, we are fitting the CFD in the real axis, which has smaller uncertainties..

As for the $f_0(980)$ resonance, we have included in the fit the pole position obtained by means of the GKPY equations in [29]. The main reason is that phenomenological fits cannot extract its accurate parameters in a very stable way (see for instance [55]). In particular, the CFD fit of [25] does not provide an accurate estimate of

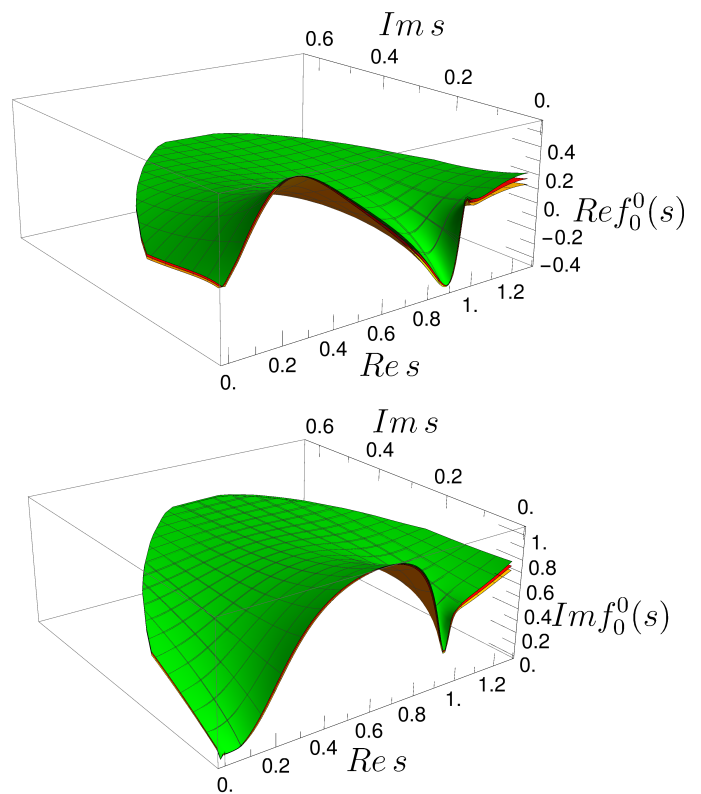


FIG. 3: Real (top) and imaginary (bottom) parts of the scalar-isoscalar partial wave in the first Riemann sheet of the complex- s plane, within the applicability region of GKPY/Roy equations. There are actually three surfaces on each plot: one for the central value, one for the upper uncertainty and another one for the lower uncertainty band. Note that the behavior of the parameterization is smooth and the uncertainties are small compared to the typical scale of the analytic structures, even deep in the complex plane. We plot solution I, but solution II is almost identical in this region.

its position and one has to rely on the numerical dispersive approach. However, with our new parameterization, the $f_0(980)$ is no longer a problem, as both the data, the cusp effect and the pole position are factored out into a simple, yet versatile functional form. Once again, the coupling of the $f_0(980)$ to $\pi\pi$ has smaller uncertainties than the GKPY determination, since the CFD partial wave, with its small uncertainty, is also fitted in the real axis to obtain our new parameterization.

Last, but not the least, the global parameterization yields relatively accurate threshold and sub-threshold parameters (like the Adler zero) compatible with those of the dispersive data analysis of the Madrid-Krakow group [25] and therefore also with the dispersive analysis matched to two-loop ChPT of the Bern group [23, 24].

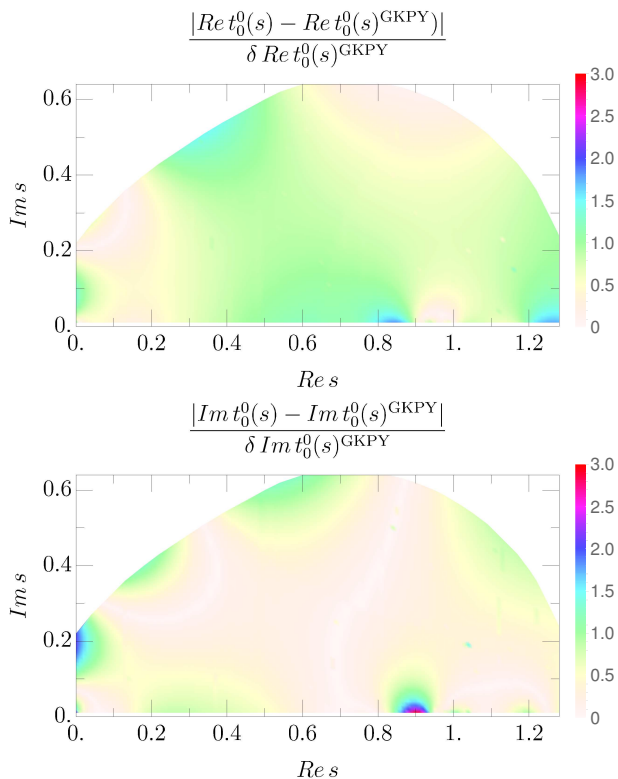


FIG. 4: Within the applicability region of GKPY equations in the complex- s plane, we show the absolute value of the differences between the real (top) and imaginary (bottom) parts of the global parameterization and the GKPY equations, divided by the uncertainty of the latter.

TABLE IV: Poles and residues of both $f_0(500)$ and $f_0(980)$ resonances. They are almost indistinguishable for Solutions I and II. The latter provides two parameters for the $t_{f_0}^0$ factor in Tables I and II. Note that they are very compatible with the GKPY dispersive results in [29].

	$\sqrt{s_{pole}}$ (MeV)	$ g $
$f_0(500)^{GKPY}$	$(457^{+14}_{-13}) - i(279^{+11}_{-7})$	$3.59^{+0.11}_{-0.13}$
$f_0(500)$	$(457 \pm 9) - i(278 \pm 7)$	3.46 ± 0.07
$f_0(980)^{GKPY}$	$(996 \pm 7) - i(25^{+10}_{-6})$	2.3 ± 0.2
$f_0(980)$	$(996 \pm 7) - i(25 \pm 8)$	2.28 ± 0.10

TABLE V: Adler zero and threshold parameters. The latter in customary $m_\pi = 1$ units. They are almost indistinguishable for Solutions I and II.

	This work	Dispersive result [25]
$\sqrt{s_{Adler}}$	96 ± 20 MeV	85 ± 34 MeV
a_0^0	0.227 ± 0.019	0.220 ± 0.008
b_0^0	0.266 ± 0.009	0.278 ± 0.005

B. P-wave fit

Following the same procedure considered for the S0 wave, in the physical region and below 1.4 GeV we will fit our parameterization to the CFD partial wave of [25]. Note that this P-wave parameterization describes data from both $\pi\pi$ scattering [4, 6, 56] and the pion vector form factor [57, 58], while fulfilling at the same time the GKPY/Roy equations up to 1.12 GeV and Forward Dispersion Relations up to 1.43 GeV. Once more, in the subthreshold region and in the complex plane we will fit the GKPY-equation dispersive results. As done for the scalar channel, we will only consider the energy region within the Lehmann ellipse, where both Roy and GKPY equations are formally valid.

Above 1.43 GeV there are no further dispersive results and hence we will only describe the available experimental data, which come from a single scattering experiment performed by the CERN-Munich Collaboration. In addition, in the vector case there is a relevant difference between the best solution of the original CERN-Munich result published in 1973 [2] and the (- - -) solution of the 1975 collaboration reanalysis [4].

The behavior of the original P-wave result shows a large interference in the region between 1.5 and 1.8 GeV. Namely, within these 300 MeV, the phase shift changes by more than 20° and the elasticity, starting from almost 1, decreases to less than 0.5 to return back to 1. This behavior could only be explained if the ρ' and ρ'' resonances and the $K\bar{K}$ channel would interfere strongly, which is in contradiction with the experimental values for the width and couplings of these two resonances [59, 60]. Thus, the solution (- - -) of Hyams 75 [4] is the one customarily used in the literature. However, we will fit both solutions for completeness, as we have done for the S0-wave. The original CERN-Munich result [2, 3] will be called solution I, whereas the fit to the updated reanalysis of [4] will be called solution II.

As previously done for the S0 wave we will fit our P-wave global parameterization described in Sec. III B to a 10 MeV-spaced grid of GKPY output values within their applicability region in the complex plane and to the CFD parameterization in the real axis at energy points separated by 5 MeV. In addition we add the $\chi^2/d.o.f.$ of the data above 1.4 GeV, although for the phase shift of both solutions we have added one degree of systematic uncertainty since the nominal uncertainties in some regions are unrealistically small, particularly for solution II. The fit minimizes a $\chi^2/d.o.f.$ function whose uncertainties are those of the GKPY or the CFD partial wave. Once more, even though our $\chi^2/d.o.f.$ does not have a well-defined statistical meaning, it ensures a nice description of the input as seen in the $\hat{\chi}^2 \equiv \chi^2/d.o.f.$ values, given in Table VI. They lie below or close to 1 in all regions (we follow the same notation as for the S0 wave).

The resulting P-wave phase shift and elasticity are plotted in Fig. 5 and their parameters are collected in Tables VII and VIII for solutions I and II, respectively.

TABLE VI: Results in terms of $\hat{\chi}^2$ of the P-wave solutions I and II, in different regions

	$\hat{\chi}_1^2$	$\hat{\chi}_2^2$	$\hat{\chi}_C^2$	$\hat{\chi}_\delta^2$	$\hat{\chi}_\eta^2$
Solution I [4]	0.6	0.4	0.6	1.3	0.8
Solution II [4]	0.6	0.5	0.7	1.2	1.2

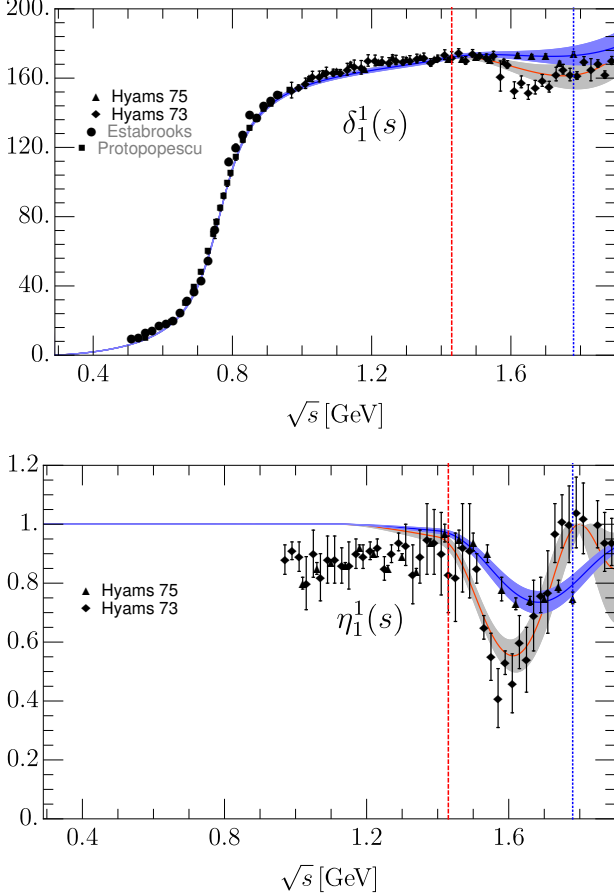


FIG. 5: Comparison of our two solutions (Table VII) with data [6] (solid squares) and [56] (solid circles). The red dashed vertical line separates the region where the fits describe data and dispersion relation results from the region above where the parameterization is just fitted to [2, 3] (solid diamonds) or to [4] (solid triangles). The blue dotted vertical line depicts the energy of the last data point of solution II. The gray band corresponds to the fit of solution I and the blue band is solution II.

Both from the figure and the tables we can see that they are almost identical up to 1.4 GeV. The uncertainties are described by the gray band for solution I and the blue band for solution II, and they are similar to those given in [25].

Concerning the region below 1.4 GeV, note that the uncertainties are extremely small below $K\bar{K}$ threshold. For this reason, and in order to ensure an accurate descrip-

TABLE VII: Fit parameters of the Global parameterization for the P-wave solution I.

	$t_{1,\text{conf}}^1$	η_1^1	$\sqrt{s} > 1.4 \text{ GeV}$	
B_0	0.97 ± 0.01	K_0 0.35 ± 0.16	d_0	11.1 ± 1.6
B_1	0.12 ± 0.03		d_1	5.6 ± 0.5
B_2	-0.18 ± 0.08		e_0	-0.146 ± 0.032
B_3	0.40 ± 0.19		e_1	0.337 ± 0.012
B_4	1.65 ± 0.39		e_2	0.198 ± 0.006
m_ρ	0.7752 ± 0.0013			

TABLE VIII: Fit parameters of the Global parameterization for the P-wave solution II.

	$t_{1,\text{conf}}^1$	η_1^1	$\sqrt{s} > 1.4 \text{ GeV}$	
B_0	0.97 ± 0.01	K_0 0.17 ± 0.05	d_0	3.6 ± 1.1
B_1	0.11 ± 0.03		d_1	2.4 ± 0.3
B_2	-0.13 ± 0.08		e_0	-0.16 ± 0.02
B_3	0.47 ± 0.19		e_1	0.043 ± 0.005
B_4	1.36 ± 0.35		e_2	0.060 ± 0.002
m_ρ	0.7752 ± 0.0013			

tion of the error band in this region, we chose $\alpha = 0.3$ in Eq. (19) so that the center of the conformal expansion in our new amplitude is close to the $\pi\pi \rightarrow \pi\pi$ threshold. In this way, the uncertainties there are dominated by the lowest conformal parameters B_0 and B_1 , ensuring that the value of the scattering length and slope parameter, given in Table X, are also consistent with the dispersive values in [25]. On the contrary, the new parameterization uncertainties close to 1.4 GeV are smaller than those quoted in [25], which is a consequence of describing simultaneously the experimental data up to 2 GeV. The P-wave elasticity in [25] is compatible with 1 below 1.12 GeV and very small below 1.4 GeV. This is why it can be reproduced by the simple polynomial parameterization given in Eq. (21).

The $\rho(770)$ -pole parameters are given in Table IX and are identical for both solutions I and II. Central values and uncertainties are nicely compatible with the dispersive results in [29].

TABLE IX: Pole and residue of the $\rho(770)$. They are almost indistinguishable for Solutions I and II. We provide the GKPY dispersive result in [29] for comparison.

	$\sqrt{s_{\text{pole}}} \text{ (MeV)}$	$ g $
$\rho(770)^{\text{GKPY}}$	$(763.7_{-1.5}^{+1.7}) - i(73.2_{-1.1}^{+1.0})$	$6.01_{-0.07}^{+0.04}$
$\rho(770)$	$(763.1 \pm 1.5) - i(73.3 \pm 1.4)$	5.99 ± 0.06

Above the matching point at 1.4 GeV the two solutions coming from the CERN-Munich experiment are incompatible among themselves. The behavior of solution I suggests a strong interference between the ρ' and ρ'' , with a sizable phase change around 1.6 GeV and a dip struc-

ture in the elasticity at the same energy. In contrast, solution II looks smoother. Namely, the phase grows slowly above 180° and the elasticity has a less pronounced dip. In addition, the uncertainties quoted in [4] are slightly smaller, which leads to a more constrained result. Nevertheless we emphasize once more that above 1.4 GeV, we consider our parameterizations purely phenomenological.

TABLE X: P-wave threshold parameters in customary $m_\pi = 1$ units. They are almost indistinguishable for Solutions I and II.

	This work	Dispersive result [25]
$a_1^1(\times 10^3)$	38.3 ± 0.6	38.1 ± 0.9
$b_1^1(\times 10^3)$	4.54 ± 0.51	5.37 ± 0.14

V. SUMMARY

In this work we have provided a global parameterization of the data for each one of the S0 and P-waves of $\pi\pi \rightarrow \pi\pi$ up to almost 2 GeV. We have made an explicit effort to keep it relatively simple in order to be easy to implement in further phenomenological and experimental analyses (in final state interactions, isobar models, etc...).

The advantages of these parameterizations are that they describe experimental data up to 2 GeV consistently with the dispersive representation in [25] and its uncertainties. In addition, they reproduce the dispersive results in the complex- s plane obtained in [29], including the poles associated to the $\sigma/f_0(500)$, $f_0(980)$ and $\rho(770)$ resonances. Moreover, their low-energy behavior is compatible with the dispersive results for the threshold parameters and the S0 Adler zero and hence with the constraints due to the QCD spontaneous chiral symmetry breaking.

Actually, these new parameterizations reproduce the

results and uncertainties of a previous piecewise fit that was constrained to satisfy Forward Dispersion relations up to 1.43 GeV and partial-wave dispersion relations (Roy and GKPY equations) up to 1.12 GeV. The latter were used in [25] to obtain a rigorous analytic continuation to the complex plane which, together with its uncertainties, is also described when continuing analytically our new parameterization, without the need for a numerical integration of the dispersion relations. This is why the pole positions and residue of the $\sigma/f_0(500)$, the $f_0(980)$ and the $\rho(770)$ are so well implemented. It also allows our parameterization to be used consistently in applications with isobar models, so popular in experimental analyses.

The new parameterizations also reproduce the existing data from 1.43 to 2 GeV, although the dispersion relations do not reach this energies. Moreover, in this region, there are two contradictory data sets, and we thus provide two solutions for each wave that describe phenomenologically either one of the conflicting sets. Nevertheless, below 1.43 GeV these two solutions agree and are consistent with the dispersive analysis.

We hope that the simplicity and the remarkable analytic properties of this data parameterization can be useful for future phenomenological and experimental studies in which $\pi\pi \rightarrow \pi\pi$ interactions are needed.

ACKNOWLEDGMENTS

JRP and AR are supported by the Spanish project FPA2016-75654-C2-2-P. This project has received funding from the European Union's Horizon 2020 research and innovation program under grant agreement No 824093. AR would also like to acknowledge the financial support of the Universidad Complutense de Madrid through a predoctoral scholarship. JRE is supported by the Swiss National Science Foundation, project No. PZ00P2_174228.

-
- [1] R. A. Briceño, J. J. Dudek, and R. D. Young, *Rev.Mod.Phys.* **90**, 025001 (2018), [arXiv:1706.06223 \[hep-lat\]](#).
- [2] B. Hyams *et al.*, *Nucl. Phys.* **B64**, 134 (1973).
- [3] G. Grayer *et al.*, *Nucl. Phys.* **B75**, 189 (1974).
- [4] B. Hyams *et al.*, *Nucl. Phys.* **B100**, 205 (1975).
- [5] R. Kaminski, L. Lesniak, and K. Rybicki, *Z. Phys.* **C74**, 79 (1997), [arXiv:hep-ph/9606362 \[hep-ph\]](#).
- [6] S. D. Protopopescu, M. Alston-Garnjost, A. Barbaro-Galtieri, S. M. Flatte, J. H. Friedman, T. A. Lasinski, G. R. Lynch, M. S. Rabin, and F. T. Solmitz, *Phys. Rev.* **D7**, 1279 (1973).
- [7] L. Rossetlet *et al.*, *Phys. Rev.* **D15**, 574 (1977).
- [8] S. Pislak *et al.* (BNL-E865), *Phys. Rev. Lett.* **87**, 221801 (2001), [Erratum: *Phys. Rev. Lett.* **105**, 019901(2010)], [arXiv:hep-ex/0106071 \[hep-ex\]](#).
- [9] J. R. Batley *et al.* (NA48-2), *Eur. Phys. J.* **C70**, 635 (2010).
- [10] J. Gasser and H. Leutwyler, *Annals Phys.* **158**, 142 (1984).
- [11] J. Gasser and H. Leutwyler, *Nucl. Phys.* **B250**, 465 (1985).
- [12] T. N. Truong, *Phys. Rev. Lett.* **61**, 2526 (1988).
- [13] A. Dobado, M. J. Herrero, and T. N. Truong, *Phys. Lett.* **B235**, 134 (1990).
- [14] A. Dobado and J. R. Pelaez, *Phys. Rev.* **D47**, 4883 (1993), [arXiv:hep-ph/9301276 \[hep-ph\]](#).
- [15] A. Dobado and J. R. Pelaez, *Phys. Rev.* **D56**, 3057 (1997),

- arXiv:hep-ph/9604416 [hep-ph].
- [16] J. A. Oller and E. Oset, *Nucl. Phys.* **A620**, 438 (1997), [Erratum: *Nucl. Phys.*A652,407(1999)], arXiv:hep-ph/9702314 [hep-ph].
- [17] J. A. Oller, E. Oset, and J. R. Pelaez, *Phys. Rev.* **D59**, 074001 (1999), [Erratum: *Phys. Rev.*D75,099903(2007)], arXiv:hep-ph/9804209 [hep-ph].
- [18] A. Gomez Nicola and J. R. Pelaez, *Phys. Rev.* **D65**, 054009 (2002), arXiv:hep-ph/0109056 [hep-ph].
- [19] J. R. Pelaez, *Mod. Phys. Lett.* **A19**, 2879 (2004), arXiv:hep-ph/0411107 [hep-ph].
- [20] J. Nieves and E. Ruiz Arriola, *Nucl. Phys.* **A679**, 57 (2000), arXiv:hep-ph/9907469 [hep-ph].
- [21] J. A. Oller and E. Oset, *Phys.Rev.* **D60**, 074023 (1999), hep-ph/9809337 [hep-ph].
- [22] K. M. Watson, *Phys. Rev.* **95**, 228 (1954).
- [23] B. Ananthanarayan, G. Colangelo, J. Gasser, and H. Leutwyler, *Phys.Rept.* **353**, 207 (2001), arXiv:hep-ph/0005297 [hep-ph].
- [24] G. Colangelo, J. Gasser, and H. Leutwyler, *Nucl. Phys.* **B603**, 125 (2001), arXiv:hep-ph/0103088 [hep-ph].
- [25] R. García-Martín, R. Kamiński, J. R. Peláez, J. Ruiz de Elvira, and F. J. Ynduráin, *Phys.Rev.* **D83**, 074004 (2011), arXiv:1102.2183 [hep-ph].
- [26] C. Ditsche, M. Hoferichter, B. Kubis, and U. G. Meissner, *JHEP* **06**, 043 (2012), arXiv:1203.4758 [hep-ph].
- [27] M. Hoferichter, J. Ruiz de Elvira, B. Kubis, and U.-G. Meißner, *Phys. Rept.* **625**, 1 (2016), arXiv:1510.06039 [hep-ph].
- [28] P. Buettiker, S. Descotes-Genon, and B. Moussallam, *Eur. Phys. J.* **C33**, 409 (2004), arXiv:hep-ph/0310283 [hep-ph].
- [29] R. García-Martín, R. Kaminski, J. R. Peláez, and J. Ruiz de Elvira, *Phys.Rev.Lett.* **107**, 072001 (2011), arXiv:1107.1635 [hep-ph].
- [30] J. R. Pelaez and F. J. Yndurain, *Phys. Rev.* **D71**, 074016 (2005), arXiv:hep-ph/0411334 [hep-ph].
- [31] R. Kaminski, J. R. Pelaez, and F. J. Yndurain, *Phys. Rev.* **D77**, 054015 (2008), arXiv:0710.1150 [hep-ph].
- [32] R. Kaminski, J. R. Pelaez, and F. J. Yndurain, *Phys. Rev.* **D74**, 014001 (2006), [Erratum: *Phys. Rev.*D74,079903(2006)], arXiv:hep-ph/0603170 [hep-ph].
- [33] F. J. Yndurain, R. Garcia-Martin, and J. R. Pelaez, *Phys. Rev.* **D76**, 074034 (2007), arXiv:hep-ph/0701025 [hep-ph].
- [34] R. Navarro Pérez, E. Ruiz Arriola, and J. Ruiz de Elvira, *Phys.Rev.* **D91**, 074014 (2015), arXiv:1502.03361 [hep-ph].
- [35] S. M. Roy, *Phys.Lett.* **36B**, 353 (1971).
- [36] I. Caprini, G. Colangelo, and H. Leutwyler, *Phys.Rev.Lett.* **96**, 132001 (2006), arXiv:hep-ph/0512364 [hep-ph].
- [37] B. Moussallam, *Eur. Phys. J.* **C71**, 1814 (2011), arXiv:1110.6074 [hep-ph].
- [38] I. Caprini, *Phys. Rev.* **D77**, 114019 (2008), arXiv:0804.3504 [hep-ph].
- [39] P. Masjuan, J. Ruiz de Elvira, and J. J. Sanz-Cillero, *Phys. Rev.* **D90**, 097901 (2014), arXiv:1410.2397 [hep-ph].
- [40] I. Caprini, P. Masjuan, J. Ruiz de Elvira, and J. J. Sanz-Cillero, *Phys. Rev.* **D93**, 076004 (2016), arXiv:1602.02062 [hep-ph].
- [41] J. R. Peláez, A. Rodas, and J. Ruiz de Elvira, *Eur. Phys. J.* **C77**, 91 (2017), arXiv:1612.07966 [hep-ph].
- [42] J. R. Pelaez and F. J. Yndurain, *Phys. Rev.* **D68**, 074005 (2003), arXiv:hep-ph/0304067 [hep-ph].
- [43] D. Atkinson, *Nucl. Phys.* **B8**, 377 (1968), [Erratum: *Nucl. Phys.*B15,331(1970)].
- [44] D. Atkinson, *Nucl. Phys.* **B23**, 397 (1970).
- [45] S. L. Adler, *Phys. Rev.* **137**, B1022 (1965), [,140(1964)].
- [46] J. Nebreda, J. R. Pelaez, and G. Rios, *Phys. Rev.* **D88**, 054001 (2013), arXiv:1205.4129 [hep-ph].
- [47] J. Pisut and M. Roos, *Nucl. Phys.* **B6**, 325 (1968).
- [48] G. D. Lafferty, *Z. Phys.* **C60**, 659 (1993).
- [49] H. Becker *et al.* (CERN-Cracow-Munich), *Argonne Symp.1978:461*, *Nucl. Phys.* **B151**, 46 (1979).
- [50] D. H. Cohen, D. S. Ayres, R. Diebold, S. L. Kramer, A. J. Pawlicki, and A. B. Wicklund, *Phys. Rev.* **D22**, 2595 (1980).
- [51] A. D. Martin and E. N. Ozmütlu, *Nucl. Phys.* **B158**, 520 (1979).
- [52] V. A. Polychronakos, N. M. Cason, J. M. Bishop, N. N. Biswas, V. P. Kenney, D. S. Rhines, R. C. Ruchti, W. D. Shephard, M. J. Stangl, and J. M. Watson, *Phys. Rev.* **D19**, 1317 (1979).
- [53] A. Etkin *et al.*, *Phys. Rev.* **D25**, 1786 (1982).
- [54] W. Wetzel, K. Freudenreich, F. X. Gentit, P. Muhlemann, W. Beusch, A. Birman, D. Websdale, P. Astbury, A. Harckham, and M. Letheren, *Nucl. Phys.* **B115**, 208 (1976).
- [55] R. A. Briceño, J. J. Dudek, R. G. Edwards, and D. J. Wilson, *Phys.Rev.* **D97**, 054513 (2018), arXiv:1708.06667 [hep-lat].
- [56] P. Estabrooks and A. D. Martin, *Nucl. Phys.* **B79**, 301 (1974).
- [57] L. M. Barkov *et al.*, *Nucl. Phys.* **B256**, 365 (1985).
- [58] S. R. Amendolia *et al.* (NA7), *Proceedings, 23RD International Conference on High Energy Physics, JULY 16-23, 1986, Berkeley, CA*, *Nucl. Phys.* **B277**, 168 (1986).
- [59] C. Hanhart, *Phys. Lett.* **B715**, 170 (2012), arXiv:1203.6839 [hep-ph].
- [60] M. Tanabashi *et al.* (Particle Data Group), *Phys.Rev.* **D98**, 030001 (2018).